

# Non-linear time series analysis of precipitation events using regional climate networks for Germany

Aljoscha Rheinwalt<sup>1,2,3</sup> · Niklas Boers<sup>1,2</sup> · Norbert Marwan<sup>1</sup> · Jürgen Kurths<sup>1,2,4,5</sup> · Peter Hoffmann<sup>1</sup> · Friedrich-Wilhelm Gerstengarbe<sup>1</sup> · Peter Werner<sup>1</sup>

Received: 11 June 2014 / Accepted: 26 April 2015 / Published online: 12 May 2015  
© Springer-Verlag Berlin Heidelberg 2015

**Abstract** Synchronous occurrences of heavy rainfall events and the study of their relation in time and space are of large socio-economical relevance, for instance for the agricultural and insurance sectors, but also for the general well-being of the population. In this study, the spatial synchronization structure is analyzed as a regional climate network constructed from precipitation event series. The similarity between event series is determined by the number of synchronous occurrences. We propose a novel standardization of this number that results in *synchronization scores* which are not biased by the number of events in the respective time series. Additionally, we introduce a new version of the network measure *directionality* that measures the spatial *directionality* of weighted links by also taking account of the effects of the spatial embedding of the network. This measure provides an estimate of heavy precipitation *isochrones* by pointing out directions along which rainfall events synchronize. We propose a climatological interpretation of this measure in terms of propagating fronts or *event traces* and confirm it for Germany by comparing our results to known atmospheric circulation patterns.

**Keywords** Rainfall · Complex networks · Precipitation events · Anisotropy · Dominant link directions · Isochrones · Event synchronization

✉ Aljoscha Rheinwalt  
aljoscha@pik-potsdam.de; rheinwalt@pik-potsdam.de

<sup>1</sup> Potsdam Institute for Climate Impact Research, P.O. Box 60  
12 03, 14412 Potsdam, Germany

<sup>2</sup> Humboldt-Universität zu Berlin, Berlin, Germany

<sup>3</sup> Potsdam University, Potsdam, Germany

<sup>4</sup> Nizhny Novgorod State University, Nizhny Novgorod,  
Russia

<sup>5</sup> University of Aberdeen, Aberdeen, UK

## 1 Introduction

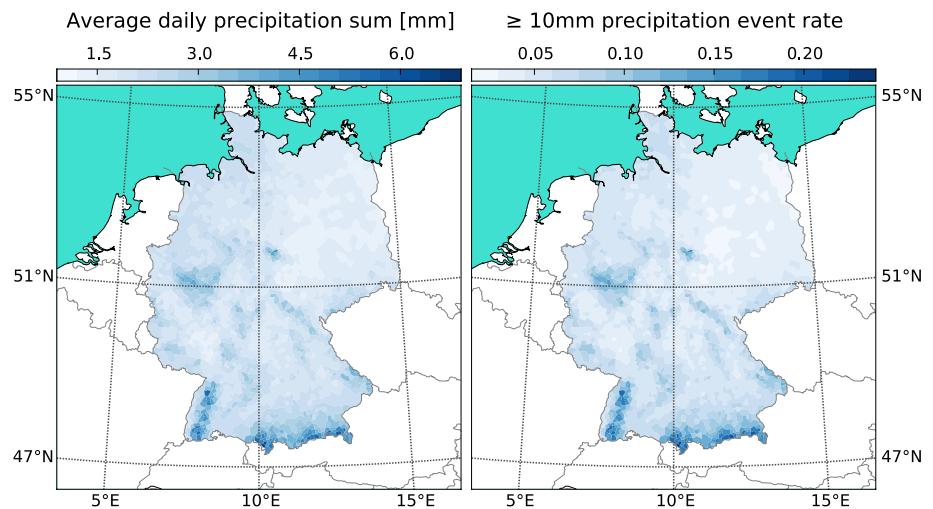
In Germany, spatial structures of precipitation are mainly determined by the orography and its position in relation to the sea. This is not only the case for long-term means of precipitation sums (Klein and Menz 2003), but holds true for heavy precipitation as well, as shown on the basis of the frequency of daily sums of 10 mm and more (Gerstengarbe and Werner 2009). As visualized in Fig. 1, large precipitation sums occur mainly in mountainous areas and in regions close to the coast of the North Sea. Small daily sums occur especially in the northeast.

In this study, our focus is exclusively on heavy precipitation in Germany, which we define as precipitation that leads to daily sums of at least 10 mm. A weather station with a daily precipitation sum larger than or equal to this threshold is considered to have a precipitation event on the corresponding day.

Variations in the spatial distribution of precipitation are well-captured by precipitation events defined by said threshold: The spatial precipitation pattern, given by average daily precipitation sums, is very similar to the spatial pattern of average event rates (see Fig. 1). Furthermore, we consider 10 mm as a good compromise between having a sufficient number of events at each location and a rather high threshold in order to study heavy precipitation. The average event rate for all event series of the entire period with a threshold of 10 mm is around 0.064. On average, we have 1300 events per event series.

In order to study synchronous occurrences of heavy precipitation events, we specify *synchronization scores* between all 2337 meteorological stations and precipitation gauges in Germany. These *scores* are defined as the number of synchronous occurrences of events in the pairs of event series, standardized to the expected number of

**Fig. 1** Average daily precipitation sums (*left*) and rates of events with precipitation  $\geq 10$  mm (*right*) for each weather station. The region of interest is decomposed into Voronoi cells with stations at cell centers. Each cell is colored according to the *colorbar* on top



synchronous occurrences assuming uniform-randomly distributed events. The obtained spatial synchronization structure is analyzed in terms of a regional climate network. Recently, similar approaches have been taken for extreme rainfall events in the Indian Monsoon System (Malik et al. 2012), as well as in the South American Monsoon System (Boers et al. 2013), but with a slightly different synchronization measure introduced by Quiroga et al. (2002) called Event Synchronization (ES). In general, applying complex network theory to climate time series has proven to deliver novel as well as established insights into climate dynamics (Paluš et al. 2011; Ebert-Uphoff and Deng 2012; Feng and Dijkstra 2014).

We will introduce a new version of the measure *directionality*, which provides *isochrones* along which heavy precipitation events typically occur synchronously. We are going to provide a climatological interpretation for this network measure, which will be confirmed by putting our results into relation with the atmospheric conditions of six important climatological circulation patterns over Germany, namely Bridge Central Europe (BM), High Central Europe (HM), Trough Central Europe (TRM), Trough Western Europe (TRW), Northwest Cyclonic (NWZ) and West Cyclonic (WZ).

## 2 Data

In this study, a precipitation gauge data set provided by the German Weather Service (Deutscher Wetterdienst) and the Potsdam Institute for Climate Impact Research is employed. It consists of 2337 daily time series for the time period 1951–2007 for Germany. Each time series consists of measurements of precipitation sums in mm/day. Since there are no missing measurements in the time period under consideration, the data is regularly sampled in time.

However, it is irregularly sampled in space. In other words, the spatial coverage of rain gauges is not homogeneous. In order to derive spatial patterns which are independent of the spatial coverage of data, we use the method proposed in Rheinwalt et al. (2012), which will be explained in the next section.

Concerning the comparison between results of this study to known atmospheric circulation patterns, we employ geopotential height at 850 hPa and corresponding wind field composites derived from the MERRA reanalysis product (Rienecker et al. 2011). This data product has a spatial resolution of  $\frac{1}{2}^\circ$  on latitudes and  $\frac{2}{3}^\circ$  on longitudes. This resolution does not resolve regional wind patterns, but still reveals large-scale atmospheric conditions. Although this daily data set starts only in 1981 it yields sufficiently accurate composites for the purpose of this study.

## 3 Methods

### 3.1 Climate networks

To analyze the spatial structure of the temporal interrelations between climate time series, climate networks have proven to be particularly useful (Tsonis et al. 2006; Donges et al. 2009; Yamasaki et al. 2008; Steinhäuser et al. 2010, 2012; Malik et al. 2012; Boers et al. 2013). Commonly, time series at different geographical locations are identified with network nodes and correlations between them are represented by network links.

Although there are studies using link-weighted climate networks (Gozolchiani et al. 2008; Steinhäuser et al. 2010; Zemp et al. 2014; Boers et al. 2014a), most focus on unweighted climate networks; especially those concerning precipitation events (Malik et al. 2012; Boers et al. 2013). In most climate networks studied so far, only the strongest

correlations between time series were represented by links. In addition, these links were typically unweighted. In contrast, we incorporate all possible links—not exclusively those corresponding to strong correlations—and weigh links according to their *synchronization score*.

The topological structure of such climate networks is assumed to encode properties of the underlying climate system. The topology is usually inspected in terms of network measures like degree, local clustering coefficient, closeness centrality, shortest-path betweenness, etc. [for instance in Boers et al. (2013)]. These node-based measures determine values for each node in space. Such a scalar or vector field of network measure values can then be visualized on a geographical map with the same spatial embedding. Features of the underlying climate network can thereby be directly related to the corresponding geographical region.

However, said network measures are known to be influenced by the spatial embedding of the network itself (Gastner and Newman 2006; Barnett et al. 2007; Henderson and Robinson 2011; Rheinwalt et al. 2012; Berezin et al. 2012). Here, networks are confined by German national borders and thus network measures experience *boundary effects* (Rheinwalt et al. 2012). Additionally, network measures are also biased by the irregular sampling of nodes in space (Heitzig et al. 2012). In this study, all these effects of the spatial embedding on network measure scores are estimated and corrected for, using the method proposed in Rheinwalt et al. (2012), but adapted for weighted networks.

### 3.2 Precipitation event series analysis

Daily precipitation time series include many zeros and comparably few spikes. Such distributions are methodologically challenging for time series analysis, since commonly used similarity measures such as Pearson’s correlation coefficient are debatable in such contexts. Here, we choose an event-based approach that standardizes the number of simultaneous events with respect to the expectation from independent time series.

For each precipitation time series we have a series of precipitation events corresponding to days with precipitation sums above the threshold of 10 mm. For each pair of such event time series, we then count how often events occur in both series at the very same time (see Fig. 2). These counts depend on the number of events. As the total number of events increases, the maximum possible number of counts also increases, as well as the number of counts that occur at random. In other words, these synchronization counts are biased by the number of events. This bias is called *event rate bias* in this study. Estimating the expected number of simultaneous events in independent time series is equivalent to the combinatorial problem of sampling without

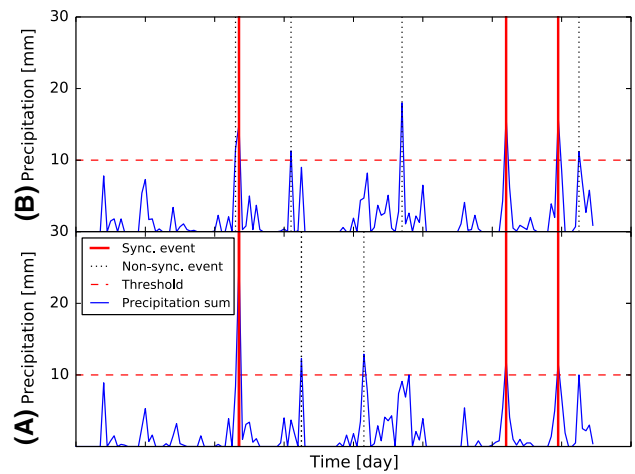


**Fig. 2** Precipitation events (vertical red and dotted black lines) are defined as days with daily precipitation sums above the 10 mm threshold (horizontal dashed red line). Events at weather station A synchronize with events at station B if they occur at the same time. These events are marked as vertical red lines

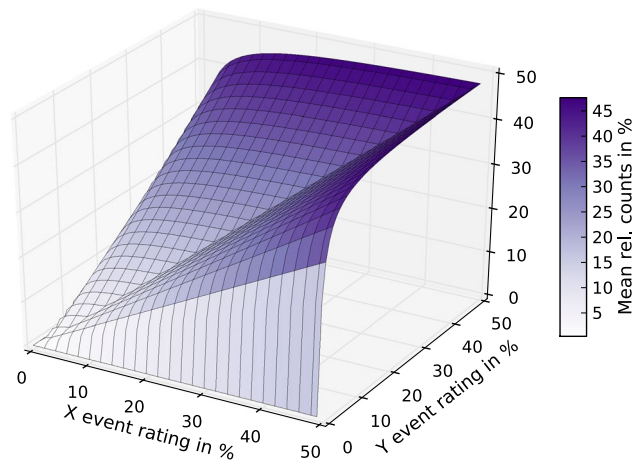


**Fig. 3** Event rate bias as a function of two random event series X and Y: We show the mean number of synchronizations in percent of the maximum possible number of synchronizations (mean rel. counts in %) given X and Y. The length of these series is 100, hence, the percentage is also the actual number of events in this example

replacement. The corresponding probability density is given by the hypergeometric distribution:

$$p(k) = \frac{\binom{y}{k} \binom{n-y}{x-k}}{\binom{n}{x}}, \tag{1}$$

where  $p(k)$  is the probability to have  $k$  synchronizations between two event series of length  $n$  with  $x$  and  $y$  events, respectively, at uniformly random time positions.

The *event rate bias* is estimated by the expected number of counts  $\langle k \rangle_p$ . The higher the event rates, the more events synchronize at random and hence, the higher is the *event rate bias*. However, no matter how high event rates are in one series, the number of synchronizations is always limited by the number of events  $y$  in the series with the lower event rate. The expected number of counts  $\langle k \rangle_p$  in percent of the maximum possible number of counts is seen in Fig. 3.

With the probability distribution  $p(k)$  (Eq. 1) obtained for the Poisson point process as a statistical model, we could test the statistical significance of synchronizations. But due to the spatial proximity of weather stations, we would reject the null hypothesis that events at two weather stations are independent of each other in more than 97 % cases with a confidence level of 99 %. Hence, setting unweighted links by significance would lead to climate networks with very high link densities.

As an alternative, we standardize synchronization counts to the distribution  $p(k)$ . Instead of using observed counts, we use the difference between observed counts and expected counts  $\langle k \rangle_p$  in units of the standard deviation of the corresponding  $p(k)$ . Hereby, the *event rate bias* in synchronization counts is eliminated and *synchronization scores* that are independent of the number of events are obtained. A *synchronization score*  $S_{ij}$  between two time series  $i$  and  $j$  is regarded as an estimate of similarity between  $i$  and  $j$ :

$$S_{ij} = \frac{k_{ij} - \langle k \rangle_p}{\sigma_p}, \tag{2}$$

where  $k_{ij}$  is the actual number of synchronous events for station  $i$  and  $j$ ,  $\langle k \rangle_p$  is the corresponding expectation value with respect to  $p(k)$ , and  $\sigma_p$  is standard deviation of the distribution  $p(k)$ . A comparison between the commonly used ES and our proposed similarity measure concerning the *event rate bias* is provided in the "Appendix".

### 3.3 Weighted climate network construction

Six weighted climate networks are examined in this study, constructed for the temporal subsets corresponding to the six dominant atmospheric circulation patterns over Germany. These networks thus represent the synchronization structure of precipitation events for the respective circulation pattern in the time period under consideration. The networks are constructed by using the corresponding matrix  $S$  of *synchronization scores* computed for the respective temporal subsets as a link-weighted network adjacency matrix.

### 3.4 Network measure

In this study, we analyze weighted climate networks with a novel version of the network measure *directionality* (Boers

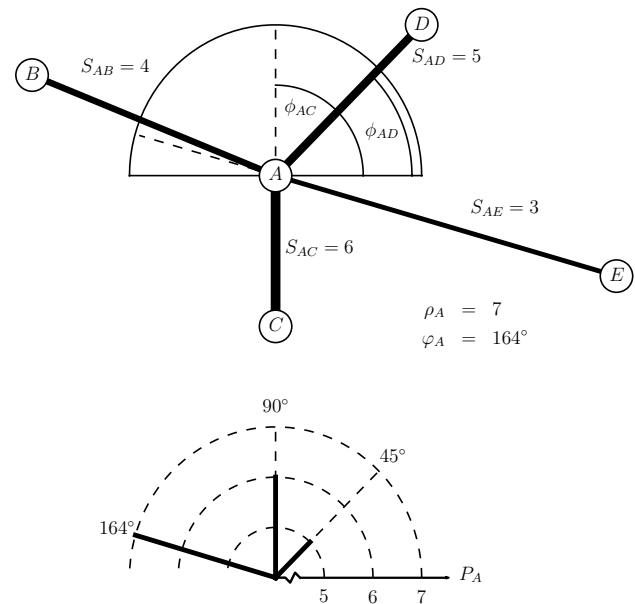


**Fig. 4** Directionality for an example node  $A$  with four neighbors  $B$ ,  $C$ ,  $D$  and  $E$ . These four neighbors result in three directions due to the fuzzy definition of angles and the network being undirected.  $\phi_{AD} = 45^\circ$  and  $\phi_{AC} = 270^\circ$  but is flipped back into the first semicircle so that  $\phi_{AC} = 90^\circ$ . The same is the case for  $\phi_{AE}$ . Therefore, also due to the fuzziness of angles, we consider  $\phi_{AB} \approx \phi_{AE} \approx 164^\circ$ . For this direction the distribution  $P_A(164^\circ) = S_{AB} + S_{AE} = 7$  which is the maximum of  $P_A$ . This results in a *directionality strength* for node  $A$  of  $\rho_A = 7$  and the tangent has an angle of  $\varphi_A = 164^\circ$

et al. 2014b), which accounts for biases in the measure due to spatial effects (Rheinwalt et al. 2012).

The *directionality* of a node  $i$  specifies a vector  $(\rho_i, \varphi_i)$  that points in the dominant direction of links concerning their number and strength. The dominant direction is derived by the mode of the frequency distribution  $P_i(\varphi)$  of synchronizations depending on the direction  $\varphi$ . The calculation of the mode is performed by using a fuzzy angle definition: A direction  $\vartheta$  is regarded as identical to  $\varphi$  if it falls into the same angle interval  $(\varphi - \epsilon, \varphi + \epsilon)$ . In this study  $\epsilon$  is chosen as 0.02 rad. Thus,  $P_i(\varphi)$  is defined as:

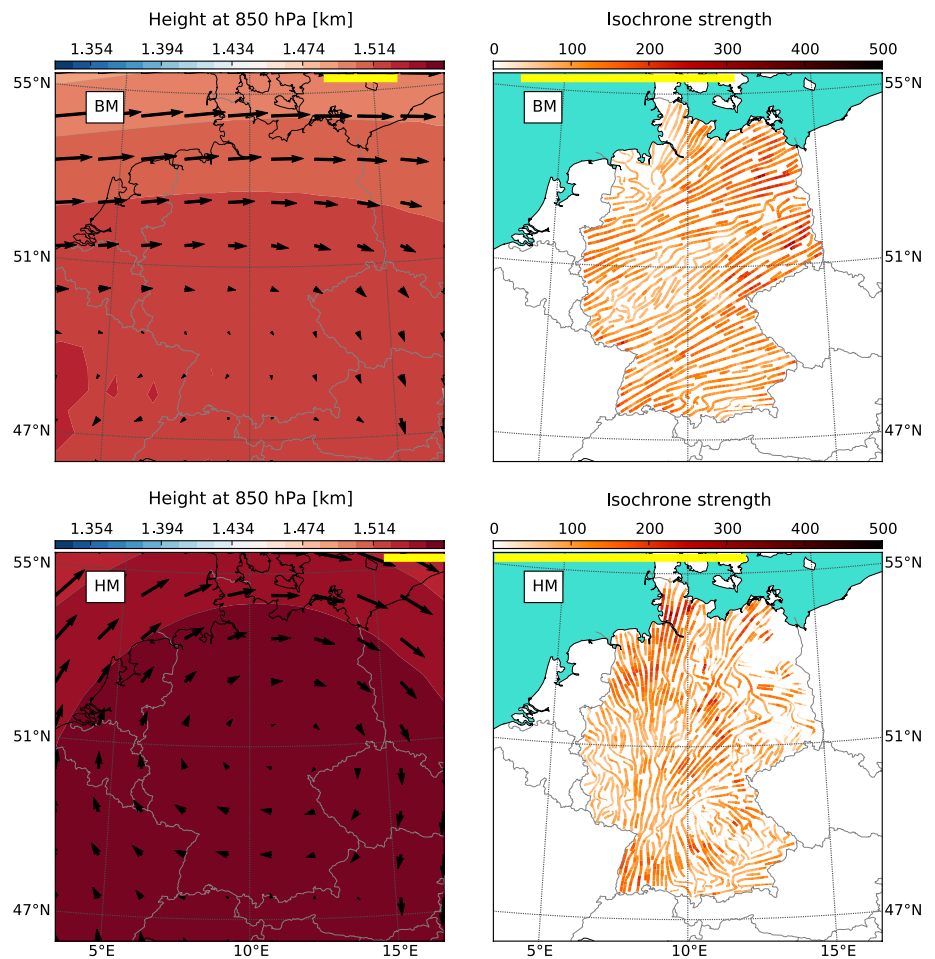
$$P_i(\varphi) = \sum_{j: \phi(i,j) \in (\varphi - \epsilon, \varphi + \epsilon)} S_{ij},$$

where  $\phi(i, j)$  denotes the angle of the link from node  $i$  to node  $j$ . Here, networks are undirected; therefore angles are projected onto the semicircle so that  $\phi(i, j) = \phi(j, i)$  (see Fig. 4 for an example). Thus,  $\varphi_i$  specifies a tangent to node  $i$ , and not a vector, along which synchronizations occur most often. The *directionality* of node  $i$  is defined as:

$$\rho_i = \max_{\varphi \in [0, \pi)} P_i(\varphi) \tag{3}$$

$$\varphi_i = \arg \max_{\varphi \in [0, \pi)} P_i(\varphi). \tag{4}$$

**Fig. 5** *Left column* geopotential height at 850 hPa and corresponding wind field composites for the low wind speed circulation patterns BM (*top*) and HM (*bottom*). *Right column* network measure *directionality*, visualized by *isochrones* for simultaneous events with color-coded values corresponding to the *directionality strength*. The line width of *isochrones* is proportional to  $1 - (\sigma^*)^2$ . Hence, more uncertain *isochrones* are thinner than more certain ones. Observe that *isochrones* are parallel to the expected orientation of fronts (as can be inferred from the composites in the *left column*). Both columns share a common *colorbar* and the range of values in a panel is marked by the corresponding *yellow bar* for that panel



Since  $P_i(\varphi)$  is not a count of links, but a count of standardized synchronizations for a given fuzzy angle  $\varphi$ , it is called a frequency distribution of synchronizations and not of links.  $\rho_i$  is regarded as the *directionality strength*.

In this study of synchronously occurring heavy precipitation events, the tangent to a node  $i$  defined by  $\varphi_i$  specifies *isochrones* for these events, i.e., lines along which events occurred simultaneously. We thus expect the *isochrones* to be typically oriented along the low-level atmospheric flow direction as determined by the corresponding wind fields. However, this may depend on the propagation speed of precipitation systems, the temporal resolution of time series and the spatial extent of the region under consideration: In case of particularly low propagation speeds in relation to the daily temporal resolution of the data, the orientation of the *isochrones* may be dominated by the actual spatial extension of the precipitation system rather than by its direction of propagation. This may happen for a slowly moving frontal system, where the *isochrones* should be expected to align with the orientation of the frontal system, and not with its direction of propagation. In contrast, fast moving precipitation systems will leave *event traces* in the

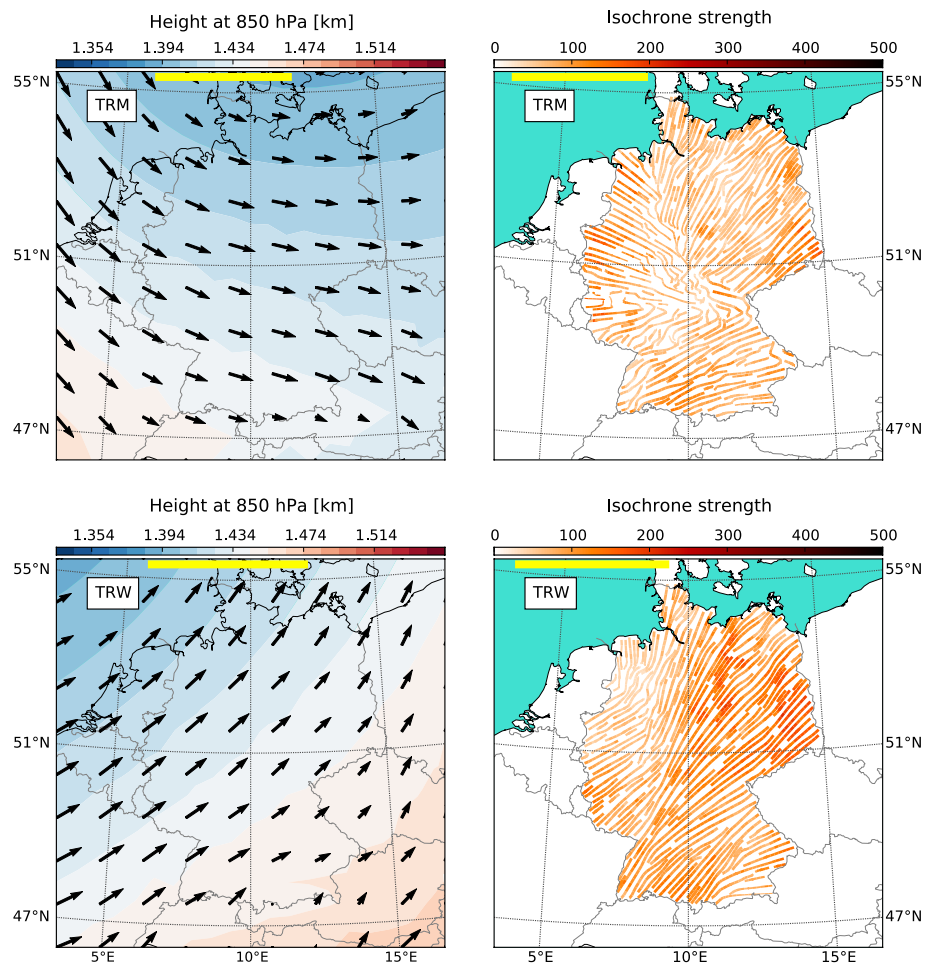
direction of the flow. If these traces are dominant, *isochrones* feature their orientation.

The measure *directionality* is visualized by coloring for each node  $i$  a tangent with angle  $\varphi_i$  according to its strength  $\rho_i$ , i.e., *isochrones* are colored by their *directionality strength* (see Figs. 5, 6, 7).

Spatial effects influencing the network measure are estimated by using a *spatial surrogate network*. Such a surrogate will be constructed such that it has the same number of nodes with the same spatial embedding as well as the same dependence of the link probability on the spatial length of links. Accordingly, the average link weight for links of a certain spatial length is the same in the original network as well as in the surrogate. This is in contrast to Rheinwalt et al. (2012), where the *spatial surrogate* was sampled by many unweighted networks in order to estimate spatial effects for unweighted network measures.

In order to correct for spatial effects in the measure *directionality*, we propose the following: The frequency distribution of synchronizations  $P_i(\varphi)$  for all nodes  $i$  is not only estimated on the original network, but also on the spatial surrogate. The *directionality* ( $\rho_i^*, \varphi_i^*$ ) of node  $i$  that

**Fig. 6** Same as Fig. 5, but for the intermediate wind speed circulation patterns TRM and TRW. Observe that for TRM *isochrones* are typically oriented in accordance with corresponding frontal systems except for the northwestern part of Germany. For the circulation pattern TRW with even faster wind speeds, *isochrones* are mostly parallel to the flow



is independent of the spatial embedding of the network is then estimated by:

$$\rho_i^* = \max_{\varphi \in [0, \pi)} P_i^{orig}(\varphi) - c_i P_i^{surr}(\varphi) \tag{5}$$

$$\varphi_i^* = \arg \max_{\varphi \in [0, \pi)} P_i^{orig}(\varphi) - c_i P_i^{surr}(\varphi). \tag{6}$$

The constant  $c_i$  is defined as the quotient of the two corresponding average frequencies of synchronizations:  $c_i = \langle P_i^{orig} \rangle / \langle P_i^{surr} \rangle$ . This re-scaling of the spatial surrogate frequency distribution of synchronizations  $P_i^{surr}(\varphi)$  ensures that the *directionality*  $(\rho_i^*, \varphi_i^*)$  is approximately the null vector if links are isotropic. However, due to the irregular sampling of nodes in space and boundaries in the network, even an isotropic link probability can lead to preferred directions of synchronizations. In other words, in such a case the frequency distribution of synchronizations  $P_i^{orig}(\varphi)$  is not necessarily flat. However, if the surrogate frequency distribution of synchronizations  $P_i^{surr}(\varphi)$  is subtracted, it does become flat since the spatial surrogate is constructed with an isotropic link probability. On the other hand, if the difference in frequency distributions has large positive

maxima at certain angles, then these are due to more synchronizations into the direction of these angles. A positive maximum at a certain fuzzy angle is therefore due to more synchronizations into that direction than what is expected from spatial effects.

In principle, a node can have multiple directions of preferred synchronizations, and our measure picks the dominant one. In order to estimate the uncertainty  $\sigma_i^*$  of this dominant direction, the weighted circular variance of all angles with positive differences in the frequency distributions of synchronizations is computed. It is defined as

$$(\sigma_i^*)^2 = \frac{\sum_{\varphi \in \Omega} w(\varphi)(\varphi - \varphi_i^*)^2}{\sum_{\varphi \in \Omega} w(\varphi)}, \tag{7}$$

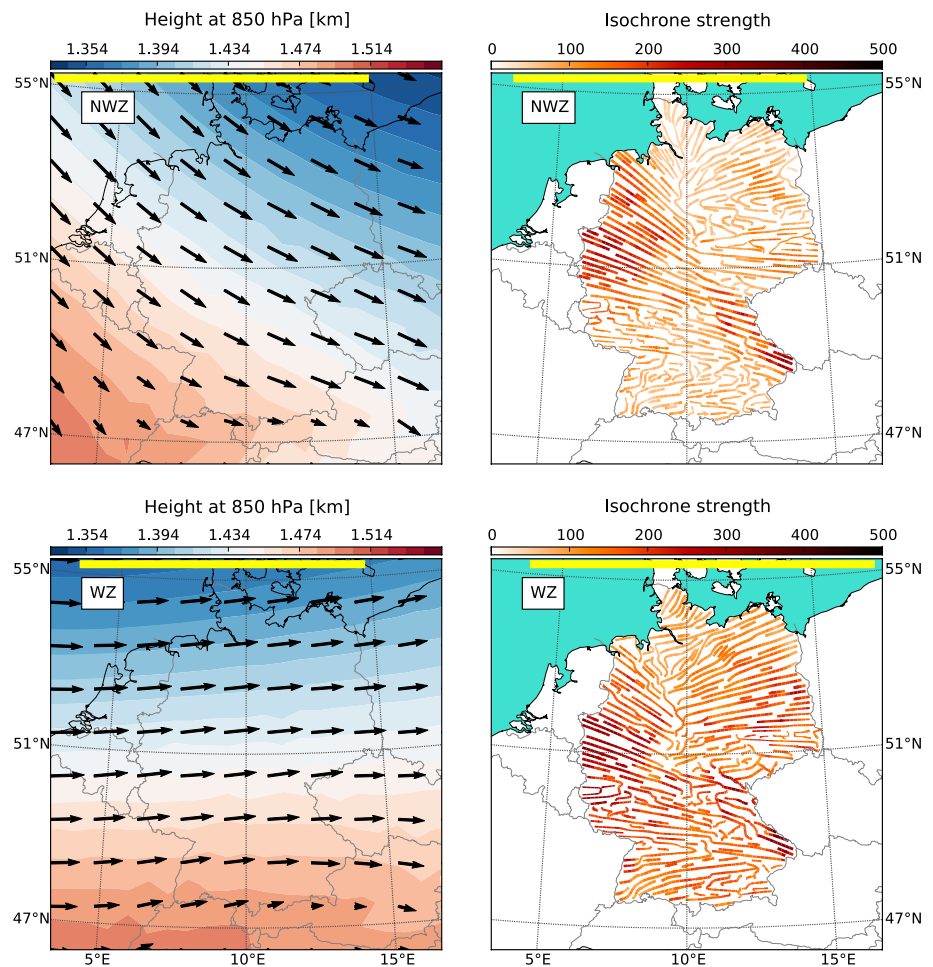
with  $\Omega = \{\varphi : w(\varphi) > 0\}$  and weights

$$w(\varphi) = P_i^{orig}(\varphi) - c_i P_i^{surr}(\varphi).$$

### 4 Results and discussion

As mentioned in the methods section above, it is expected that *isochrone* patterns for precipitation are strongly determined

**Fig. 7** Same as Fig. 5, but for the intermediate wind speed circulation patterns NWZ and WZ. Note that except for orographic perturbations *isochrones* are overall parallel to the wind flow at 850 hPa



by the flow direction of air masses. Here, the influence of atmospheric circulation patterns on the orientation of *isochrones* and values of the *directionality strength* is assessed by reference to six of the most frequent circulation patterns according to Hess and Brezowsky (Werner and Gerstengarbe 2010): two rather dry patterns with low wind speeds (BM and HM, Fig. 5), two with intermediate wind speeds but high importance for long lasting rainfall that is likely to lead to floods (Mudelsee et al. 2004) (TRM and TRW, Fig. 6), and the most frequent circulation patterns with high wind speeds (NWZ and WZ, Fig. 7). For each circulation pattern the novel network measure is compared to a composite of geopotential height and wind at 850 hPa. Note that the geopotential height fields are on the same scale in Figs. 5, 6, and 7, while the length of the wind arrows are not comparable among figures. Since wind speeds are proportional to the margin between the isobars, they can thus still be compared qualitatively.

#### 4.1 Low wind speeds (Fig. 5)

The circulation pattern BM with bridge-like highs over Central Europe leads to a relatively slow eastward movement of

northwest-to-southwest fronts over Germany (Werner and Gerstengarbe 2010). If such fronts cause precipitation events, these events propagate slowly and are hence expected to lead to *isochrones* that are parallel to the orientation of fronts.

The circulation pattern HM is even drier than BM, especially in the northeast of Germany, where precipitation events do not synchronize significantly enough along a dominant direction. For this pattern, *isochrones* exhibit rather high uncertainty in some geographical regions, and are hence very thin or even nonexistent in these areas. With anticyclones located over the middle of Germany, the circulation pattern HM favors clockwise, slow circulations of frontal systems (Werner and Gerstengarbe 2010). In accordance with our climatological interpretation, this leads to an *isochrone* pattern with *isochrones* typically oriented perpendicularly to the circulation direction. However, this pattern is rather perturbed. This may be explained by the strong influence of orography on precipitation: For instance in the Bavarian Alps (BA in Fig. 8), *isochrones* are parallel to the mountain range of the Alps. Also the Rhenish Massif (RM in Fig. 8) and the Rhineland-Palatinate (RP in Fig. 8) perturb the *isochrone* pattern.

## 4.2 Intermediate wind speeds (Fig. 6)

From the geopotential height and wind composites obtained for the circulation pattern TRM, a southwest–northeast orientation of frontal systems can be inferred. In most parts of Germany, the corresponding *isochrones* are aligned with this orientation, suggesting that they are caused by rather slowly moving fronts. The exception to this is the north-western part of Germany, where *isochrones* are rather parallel to the flow. This might be explainable by the fact that wind speeds over this region are higher than over the remaining parts of Germany, resulting in *isochrones* along the propagation direction of precipitation systems. This change in the orientation of the *isochrones* is very abrupt and can be expected to be associated with the influence of orography. For instance, the influence of the Thuringian

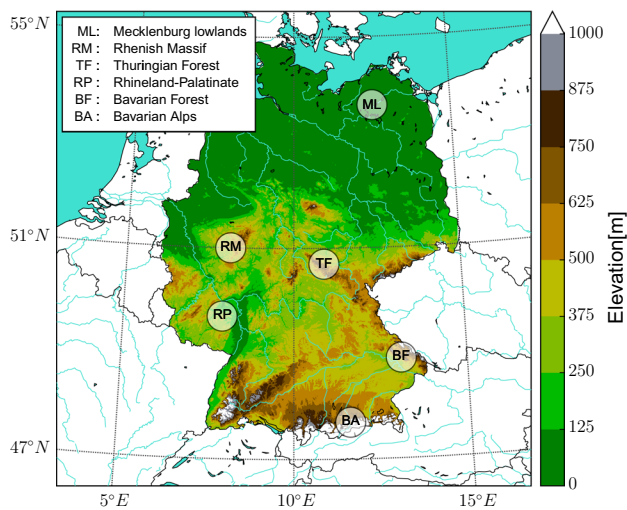
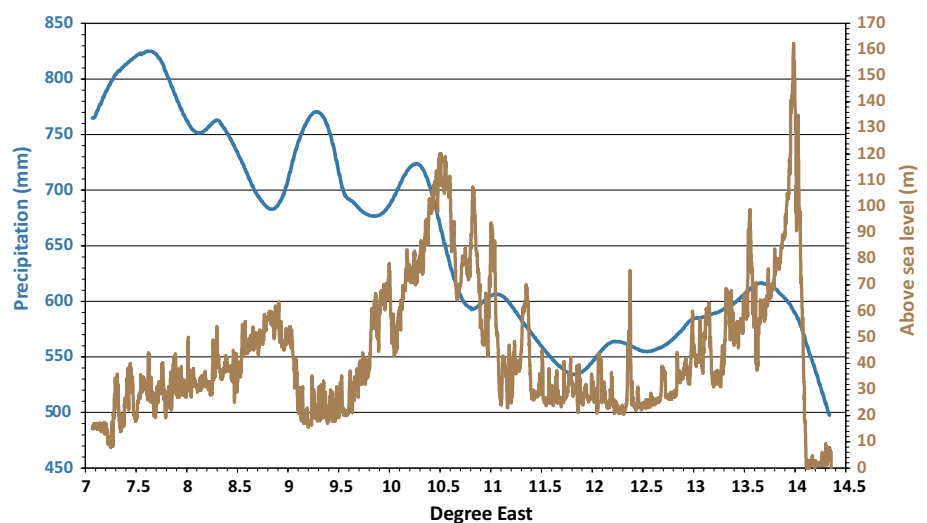


**Fig. 8** Orographic map of Germany showing regions to which this study refers to by name

**Fig. 9** Yearly precipitation in blue and above-sea-level altitude in brown along the 52.75°N line of latitude



Forest (TF in Fig. 8) on *isochrones* is very pronounced in this circulation pattern.

For the circulation pattern TRW, *isochrones* are oriented along *event traces* and therefore parallel to the orientation of the flow, in accordance with our interpretation given in Sect. 3.4.

## 4.3 High wind speeds (Fig. 7)

For the circulation pattern NWZ, relatively strong *isochrones* are observed. Note the dark red *isochrones* in the northwest of Germany and along the mountain range from the Thuringian Forest (TF in Fig. 8) to the Bavarian Forest (BF in Fig. 8). All strong *isochrones* are parallel to the wind flow at 850 hPa. Especially in the northeast of Germany, *isochrones* are rather weak, and as for TRM, the orientation of *isochrones* changes abruptly approximately along the 10°E line of longitude. The reason for this abrupt change in orientation might be an orographic barrier at  $\approx 10^\circ\text{E}$  (see Fig. 9). The influence of this barrier on yearly precipitation sums is seen in Fig. 9, which depicts the orography and precipitation distribution alongside the 52.75°N line of latitude. One can see that the terrain ascends from approximately 9.5°E–10.5°E from 20 m to 120 m above sea level, before descending again towards the Mecklenburg lowlands (ML in Fig. 8). Parallel to this, precipitation drops from 740 mm/year at 10.5°E to only 550 mm/year at 11.5°E.

This sudden change in *isochrone* orientation in the north of Germany can also be observed for the circulation pattern WZ. However, in this case the *directionality strength* in the northeast of Germany is higher than for NWZ and more parallel to the wind flow. Also, *isochrones* in the mountainous South of Germany are less perturbed by orography and thus more in accordance with the flow direction for WZ than for NWZ.

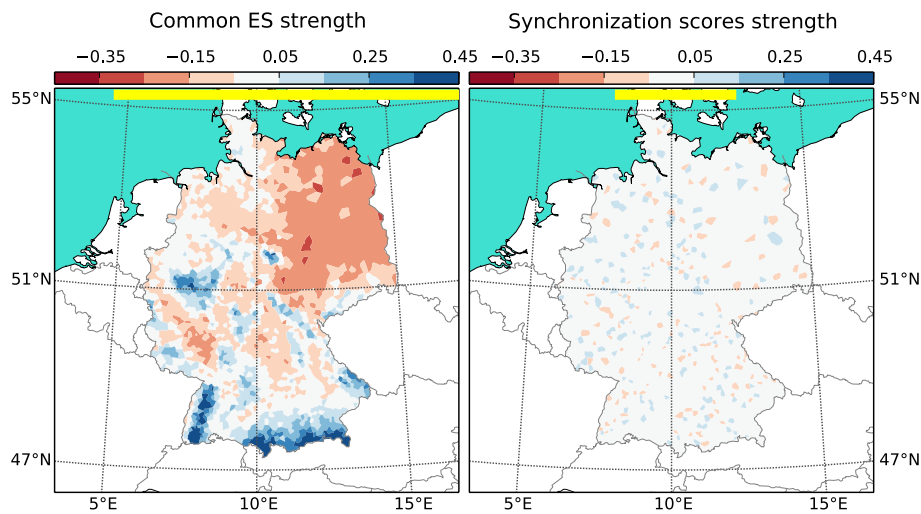


**Fig. 10** Network measure *strength* for two weighted networks constructed from the same random event series of length 1000, but using a different similarity measure. The left weighted network is constructed using the common ES and the right one using our proposed standardization of synchronization counts. The number of random events in a time series corresponds to the actual event rate found in

observations for these stations [(see Fig. 1 (right))]. The commonly used ES (left) is biased by the event rate and replicates the intensity pattern as seen in Fig. 1. Our proposed *synchronization scores* (right) show a weak random strength field. The left and right panels have the same *colorbar* and the actual range of values for a panel is given by the corresponding *yellow bar*

## 5 Conclusion

Based on long-term gauge station data with high spatial resolution, we investigated the spatial characteristics of daily heavy precipitation synchronicity in Germany by means of complex networks. We introduced a new version of the network measure *directionality* that accounts for spatial effects in weighted climate networks, discussed its applicability on regional scales and provided climatological interpretations. This measure provides insights into the climatological orientation of the propagation of precipitation clusters and frontal systems in terms of *isochrones* which, while being consistent with known circulation patterns, go beyond the hitherto known. The presented methodology also provides a promising framework for evaluating climate models with respect to their implementation regarding heavy precipitation. Furthermore, we are convinced that our findings can be helpful for the assessment of hazard risks in form of floodings and, if combined with climate model projections, the development of these risks under ongoing climate change.

**Acknowledgments** This study was supported by the Deutsche Forschungsgemeinschaft (DFG), project MA 4759/4-1, and the International Research Training Group (IRTG) 1740/TRP 2011/50151-0 that is co-funded by the DFG and the Foundation for Research Support of the State of Sao Paulo (FAPESP).

## Appendix: Comparison between the commonly used ES and our proposed similarity measure concerning the *event rate bias*

The commonly used ES introduced as by Quiroga et al. (2002) uses synchronization counts normalized by  $\sqrt{x \cdot y}$ , where  $x$  and  $y$  are the number of events in each time series. But in order to obtain a notion of synchronicity that is independent of the number of events, this does not suffice.

The local node-based network measure *strength*  $s_i$  of a node  $i$  is defined as the sum of all its link weights:  $s_i = \sum_j S_{ij}$ . Hence,  $s_i$  gives an estimate on how well heavy precipitation at a given weather station  $i$  is synchronized to heavy precipitation at all other weather stations.

In Fig. 10 we compare this measure of two artificial networks. Both networks are constructed from the same set of random event series, but using a different similarity measure for each network. Note the relevance of the bias by the event rate for this study concerning the spatial pattern of network measures.

## References

- Barnett L, Di Paolo E, Bullock S (2007) Spatially embedded random networks. *Phys Rev E* 76:056115. doi:[10.1103/PhysRevE.76.056115](https://doi.org/10.1103/PhysRevE.76.056115)

- Berezin Y, Gozolchiani A, Guez O, Havlin S (2012) Stability of climate networks with time. *Sci Rep* 2:666
- Boers N, Bookhagen B, Marwan N, Kurths J, Marengo J (2013) Complex networks identify spatial patterns of extreme rainfall events of the South American monsoon system. *Geophysical Research Letters* 40(16):4386
- Boers N, Bookhagen B, Barbosa H, Marwan N, Kurths J, Marengo J (2014a) Prediction of extreme floods in the eastern central andes based on a complex networks approach. *Nat Commun* 5:5199
- Boers N, Rheinwalt A, Bookhagen B, Barbosa HMJ, Marwan N, Marengo J, Kurths J (2014b) The South American rainfall dipole: a complex network analysis on extreme events. *Geophys Res Lett* 41:7397
- Donges J, Zou Y, Marwan N, Kurths J (2009) The backbone of the climate network. *Europhys Lett* 87:48007
- Ebert-Uphoff I, Deng Y (2012) A new type of climate network based on probabilistic graphical models: results of boreal winter versus summer. *Geophys Res Lett* 39(19):L19701
- Feng QY, Dijkstra H (2014) Are North Atlantic multidecadal SST anomalies westward propagating? *Geophys Res Lett* 41(2):541–546
- Gastner M, Newman M (2006) The spatial structure of networks. *Eur Phys J B* 49(2):247
- Gerstengarbe FW, Werner P (2009) Klimaextreme und ihr Gefährdungspotential für Deutschland. *Geographische Rundschau* 9:12
- Gozolchiani A, Yamasaki K, Gazit O, Havlin S (2008) Pattern of climate network blinking links follows El Niño events. *EPL Europhys Lett* 83(2):28005
- Heitzig J, Donges J, Zou Y, Marwan N, Kurths J (2012) Node-weighted measures for complex networks with spatially embedded, sampled, or differently sized nodes. *Eur Phys J B Condens Matter Complex Syst* 85(1):1
- Henderson J, Robinson P (2011) Geometric effects on complex network structure in the cortex. *Phys Rev Lett* 107(1):18102
- Klein D, Menz G (2003) Niederschlag im Jahresverlauf. Klima, Pflanzen und Tierwelt. In: Institut für Länderkunde: Nationalatlas der Bundesrepublik Deutschland. Leipzig
- Malik N, Bookhagen B, Marwan N, Kurths J (2012) Analysis of spatial and temporal extreme monsoonal rainfall over South Asia using complex networks. *Climate dynamics* 39(3–4):971
- Mudelsee M, Börngen M, Tetzlaff G, Grünwald U (2004) Extreme floods in central Europe over the past 500 years: Role of cyclone pathway Zugstrasse Vb. *J Geophys Res Atmos* (1984–2012) 109(D23):D23101
- Paluš M, Hartman D, Hlinka J, Vejmelka M (2011) Discerning connectivity from dynamics in climate networks. *Nonlinear Process Geophys* 18:751
- Quiroga R, Kreuz T, Grassberger P (2002) Event synchronization: a simple and fast method to measure synchronicity and time delay patterns. *Phys Rev E* 66(4):041904
- Rheinwalt A, Marwan N, Kurths J, Werner P, Gerstengarbe FW (2012) Boundary effects in network measures of spatially embedded networks. *EPL* 100(2):28002
- Rienecker MM, Suarez MJ, Gelaro R, Todling R, Bacmeister J, Liu E, Bosilovich MG, Schubert SD, Takacs L, Kim GK, Bloom S, Chen J, Collins D, Conaty A, Da Silva A, Gu W, Joiner J, Koster RD, Lucchesi R, Molod A, Owens T, Pawson S, Pegion P, Redder CR, Reichle R, Robertson FR, Ruddick AG, Sienkiewicz M, Woollen J (2011) MERRA: NASA's Modern-Era retrospective analysis for research and applications. *J Clim* 24:3624. doi:10.1175/JCLI-D-11-00015.1
- Steinhaeuser K, Chawla N, Ganguly A (2010) An exploration of climate data using complex networks. *ACM SIGKDD Explor Newsl* 12(1):25
- Steinhaeuser K, Ganguly AR, Chawla NV (2012) Multivariate and multiscale dependence in the global climate system revealed through complex networks. *Clim Dyn* 39(3–4):889. doi:10.1007/s00382-011-1135-9
- Tsonis A, Swanson K, Roebber P (2006) What do networks have to do with climate? *Bull Am Meteorol Soc* 87(5):585
- Werner P, Gerstengarbe F (2010) Katalog der Großwetterlagen Europas (1881–2009) nach Paul Hess und Helmut Brezowsky. Potsdam Institut für Klimafolgenforschung, Potsdam
- Yamasaki K, Gozolchiani A, Havlin S (2008) Climate networks around the globe are significantly affected by El Niño. *Phys Rev Lett* 100(22):228501
- Zemp D, Wiedermann M, Kurths J, Rammig A, Donges J (2014) Node-weighted measures for complex networks with directed and weighted edges for studying continental moisture recycling. *EPL Europhys Lett* 107(5):58005